# 1 The impact of phage and phage resistance on microbial

# **2** community dynamics

- 3 Ellinor O Alseth<sup>1,2,3</sup>¶\*, Rafael Custodio<sup>1</sup>¶, Sarah A Sundius<sup>2,4,5</sup>, Rachel A Kuske<sup>2,4</sup>, Sam P.
- 4 Brown<sup>2,3&</sup>, Edze R Westra<sup>1&</sup>

5

- <sup>1</sup>Environment and Sustainability Institute, Biosciences, University of Exeter, Penryn, UK
- <sup>2</sup>Center for Microbial Dynamics and Infection, Georgia Institute of Technology, Atlanta,
- 8 Georgia, USA
- <sup>9</sup> School of Biological Sciences, Georgia Institute of Technology, Atlanta, Georgia, USA
- <sup>4</sup>School of Math, Georgia Institute of Technology, Atlanta, Georgia, USA
- <sup>5</sup>Interdisciplinary Program in Quantitative Biosciences, Georgia Institute of Technology,
- 12 Atlanta, Georgia, USA

13

- \* Corresponding author
- 15 E-mail: ealseth3@gatech.edu (EOA)

- 17 These authors contributed equally to this work.
- 18 & These authors also contributed equally to this work.

### **Abstract**

19

20

21

22

23

24

25

26

27

28

29

30

31

32

33

34

35

36

37

38

39

40

41

Where there are bacteria, there will be bacteriophages. These viruses are known to be important players in shaping the wider microbial community in which they are embedded, with potential implications for human health. On the other hand, bacteria possess a range of distinct immune mechanisms that provide protection against bacteriophages, including the mutation or complete loss of the phage receptor, and CRISPR-Cas adaptive immunity. While our previous work showed how a microbial community may impact phage resistance evolution, little is known about the inverse, namely how interactions between phages and these different phage resistance mechanisms affect the wider microbial community in which they are embedded. Here, we conducted a 10-day, fully factorial evolution experiment to examine how phage impact the structure and dynamics of an artificial four-species bacterial community that includes either *Pseudomonas aeruginosa* wild type or an isogenic mutant unable to evolve phage resistance through CRISPR-Cas. Additionally, we used mathematical modelling to explore the ecological interactions underlying full community behaviour, as well as to identify general principles governing the impacts of phage on community dynamics. Our results show that the microbial community structure is drastically altered by the addition of phage, with Acinetobacter baumannii becoming the dominant species and P. aeruginosa being driven nearly extinct, whereas P. aeruginosa outcompetes the other species in the absence of phage. Moreover, we find that a P. aeruginosa strain with the ability to evolve CRISPR-based resistance generally does better when in the presence of A. baumannii, but that this benefit is largely lost over time as phage is driven extinct. Finally, we show that pairwise data alone is insufficient when modelling our microbial community, both with and without phage, highlighting the importance of higher-order interactions in governing multi-species dynamics in complex communities. Combined, our data clearly illustrate how phage targeting a dominant species allows for the competitive release of the strongest competitor whilst also contributing to community diversity maintenance and potentially preventing the reinvasion of the target species, and underline the importance of mapping community composition before therapeutically applying phage.

## Introduction

Microbiome research is a dynamic and growing field in microbiology, producing an incredible amount of sequence data from a wide range of clinical and environmental samples. Humans, for instance, are colonised by a large number of microorganisms and research continues to implicate microbial communities as potential drivers behind multiple important biological processes [1–3]. These processes may play important roles in human health and disease, with some work focusing on correlations based on microbiome composition [4–8] while other look more closely for direct causality [9–12]. Still, the challenge to move beyond descriptive and correlative approaches remains, and there is a need to develop bottom-up mechanistic and quantitative understanding of the forces acting upon and shaping microbial communities. To this end, synthetic polymicrobial communities are being designed, and are gaining traction in both pure and applied microbiome studies [13–16]. Synthetic microbiomes allow for precise and malleable experimental testing of the basic rules that govern both microbial organisation and functioning on molecular and ecological scales [17–20], as well as allowing for exploration

of causal roles connecting specific microbiome structures to potential outcomes of interest.

66

67

68

69

70

71

72

73

74

75

76

77

78

79

80

81

82

83

84

85

86

64

65

Bacteria and their viral predators, bacteriophages (phages), have long been of interest in microbiological research, in part due to being the most abundant biological entity on the planet [21,22]. Phages are highly diverse in terms of their morphology, genetics, and life histories [21,23], with a clear distinction between obligatory killing lytic phages and temperate phages that can either cause a dormant infection (lysogenic cycle) or cell lysis to release new phage particles (lytic cycle). Phages are thought to play a key role in shaping both the taxonomic and functional composition of microbial communities as well as their stability, ecology and evolution [23–27]. For example, lytic replication will per definition cause a reduction in the density of the bacterial host strain or species, which in turn can have knock-on effects for the microbial community composition through the enabling of invasion and/or co-existence of competitor species. Despite the large potential impact of lytic phage, only a very limited number of experimental studies have explored the ecology and evolution of bacteria-phage interactions in a microbial community context [28,29], and it remains unclear if and how interactions between different species in more complex communities shape the effects of lytic phages on microbial eco-evolutionary dynamics. Consequently, we lack the stepping stones to understand how phages shape microbial community dynamics (reviewed in [23]), which are urgently needed to understand potentially causal relationships between natural phage communities and a variety of human diseases [30-35], and for optimising the therapeutic application of phages in the clinic.

A key consideration in this context is that bacteria can overcome phage infection through a range of different means [36,37], with varied underlying molecular mechanisms and which can act during different stages of phage infection [38–41]. Through the modification, masking or complete loss of phage-binding surface receptors for example, bacteria can prevent phage adsorption and injection [40,42]. Systems such as CRISPR-Cas on the other hand work by inserting short DNA sequences from phage and other invasive mobile genetic elements into the host genome to provide future immunological memory [43]. Unlike CRISPR-based resistance [15], phage resistance through receptor mutation can be associated with substantial phenotypic shifts and fitness trade-offs, through changes to virulence [44,45], biofilm formation [46], or antibiotic resistance [47].

While our previous work asked how interspecific competition shapes phage resistance evolution in *P. aeruginosa* [15], we here sought to answer the inverse and complimentary question of how host-phage interactions shape the composition and stability of the wider microbial community. To this end, we combined exploratory and hypothesis driven approaches, applying experimental evolution to examine how a phage impacts the dynamics of an artificial bacterial community. This community consisted of *Pseudomonas aeruginosa*, *Staphylococcus aureus*, *Acinetobacter baumannii*, and *Burkholderia cenocepacia*, all of which are opportunistic pathogens that can cause severe infection and may co-infect with one another [48–51]. Firstly, we hypothesised that the addition of a *P. aeruginosa* specific phage would promote species coexistence by limiting *P. aeruginosa* dominance through competitive release (expansion of phage resistant

competitors, following removal of phage susceptible competitor) in a way akin to what is commonly observed with antibiotics [14,52–55]. Secondly, we hypothesised that blocking the ability of *P. aeruginosa* to evolve CRISPR-based immunity would reduce *P. aeruginosa* persistence due to community dependent fitness costs of surface-modification [15]. Finally, we asked if we could quantitatively capture community dynamics using mathematical modelling. We found that the addition of a *P. aeruginosa* targeting phage resulted in the general maintenance of community diversity and coexistence, but also a shift in dominant species from *P. aeruginosa* to *A. baumannii* — with the former being unable to reinvade even after the phage was driven extinct. The impact of the type of phage resistance was limited or transient, however: While a *P. aeruginosa* wild-type with the ability to evolve CRISPR-based phage resistance initially had a slight fitness advantage in the presence of *A. baumannii* over its CRISPR-negative isogenic mutant, this effect was lost over time as the phage was driven extinct.

## **Results**

To measure the effect of phage on microbial community dynamics, we carried out a fully factorial 10-day *in vitro* evolution experiment using all possible combinations of one, two, three or four competitor species: *S. aureus*, *A. baumannii*, *B. cenocepacia*, and *P. aeruginosa* PA14 in the presence or absence of lytic phage DMS3vir. We previously applied the same model community to explore the effect of interspecific competition on phage resistance evolution in the *P. aeruginosa* wild-type (WT) over 3 days in the presence of phage [15]. Here, we include both the WT *P. aeruginosa* PA14 strain, which can evolve CRISPR-based phage resistance, and an isogenic mutant lacking a functional

CRISPR system to examine the impact of CRISPR-Cas vs surface modification on these dynamics. Following inoculation, we tracked the microbial community dynamics for all experimental treatments at regular intervals over a period of 10 days. All experiments were conducted in Lysogeny Broth (LB) at 37°C (see methods for details).

# P. aeruginosa dominates in the absence of phage

Without *P. aeruginosa* present in the community, *S. aureus* was primarily the dominant species – with the ability to co-exist with *A. baumannii* while outcompeting *B. cenocepacia* (Figs 1 and S1). This, however, was not reflected once *P. aeruginosa* was introduced to the community. In the absence of phage, *P. aeruginosa* quickly became the dominant species in the microbial community, regardless of starting composition and the *P. aeruginosa* genotype (PA14 WT vs CRISPR-KO) (Figs 2 and S3). Consistent with this, the densities of the competitor species rapidly declined during these co-culture experiments (Fig 2). Yet there was a clear difference in the rate at which competitor species declined in frequency, which was highest for *S. aureus* and lowest for *A. baumannii* (Fig 2, ANOVA: effect of treatment on *S. aureus*; F = 2.2, P = 0.09; overall model fit; adjusted P = 0.52, P = 0.67; overall model fit; adjusted P = 0.66, P = 0.52, P = 0.67; overall model fit; adjusted P = 0.66; overall model fit; adjusted P

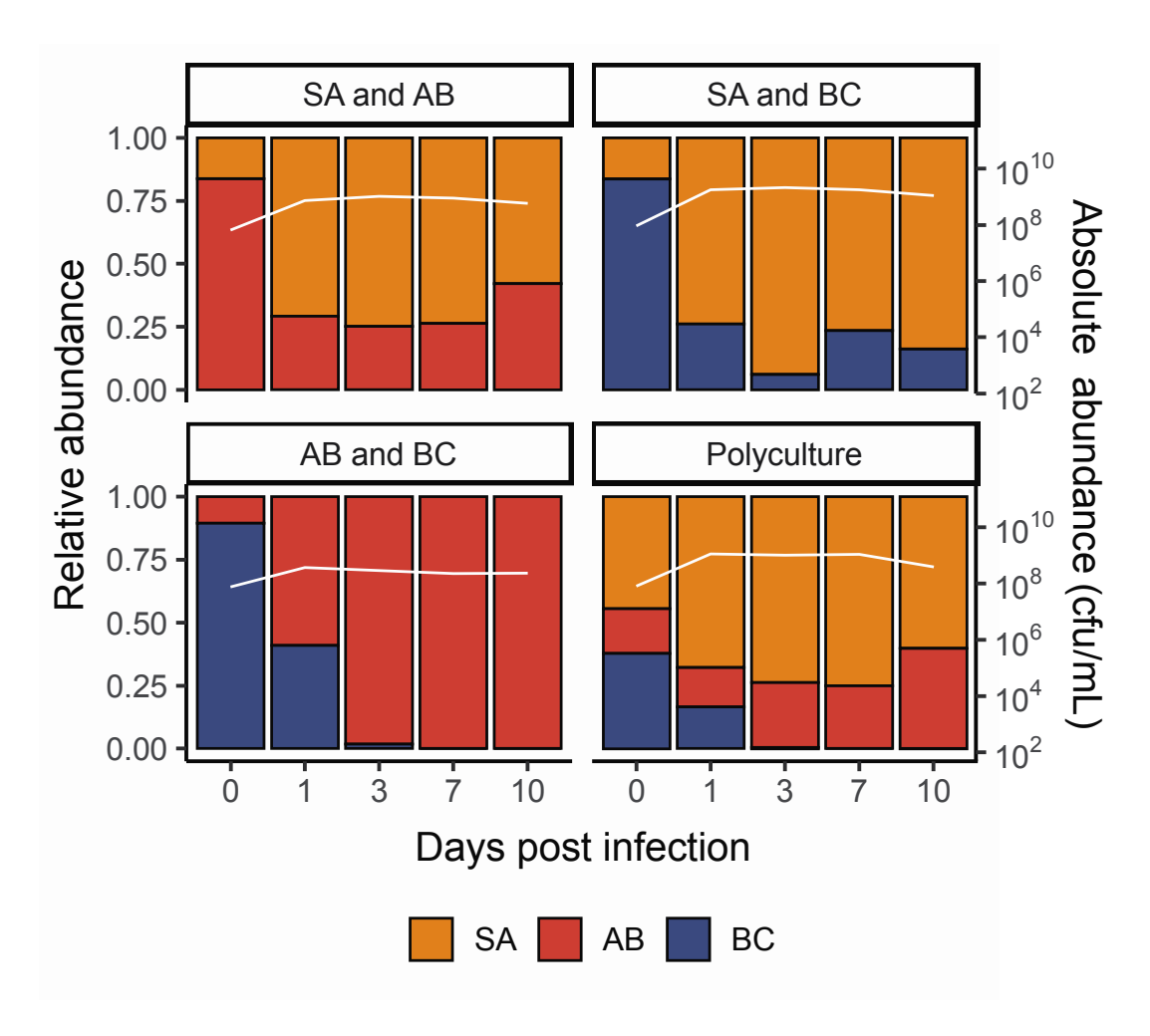


**Fig 1.** *S. aureus* and *A. baumannii* both perform well in the absence of P. aeruginosa. Showing the community composition and bacterial densities in cfu/mL over time for the microbial communities in the absence of *P. aeruginosa*. The community composition was estimated by qPCR at days 0, 1, 3, 7 and 10 of the experiment. The coloured bars represent the relative abundance of each species (left y axis), while the white line represents total abundance in cfu/mL (right y axis). Each panel represents average composition across six replicates for each treatment over time. SA = *S. aureus*, AB = *A. baumannii*, BC = *B. cenocepacia*. For individual replicates of species abundance, see Fig. S1.

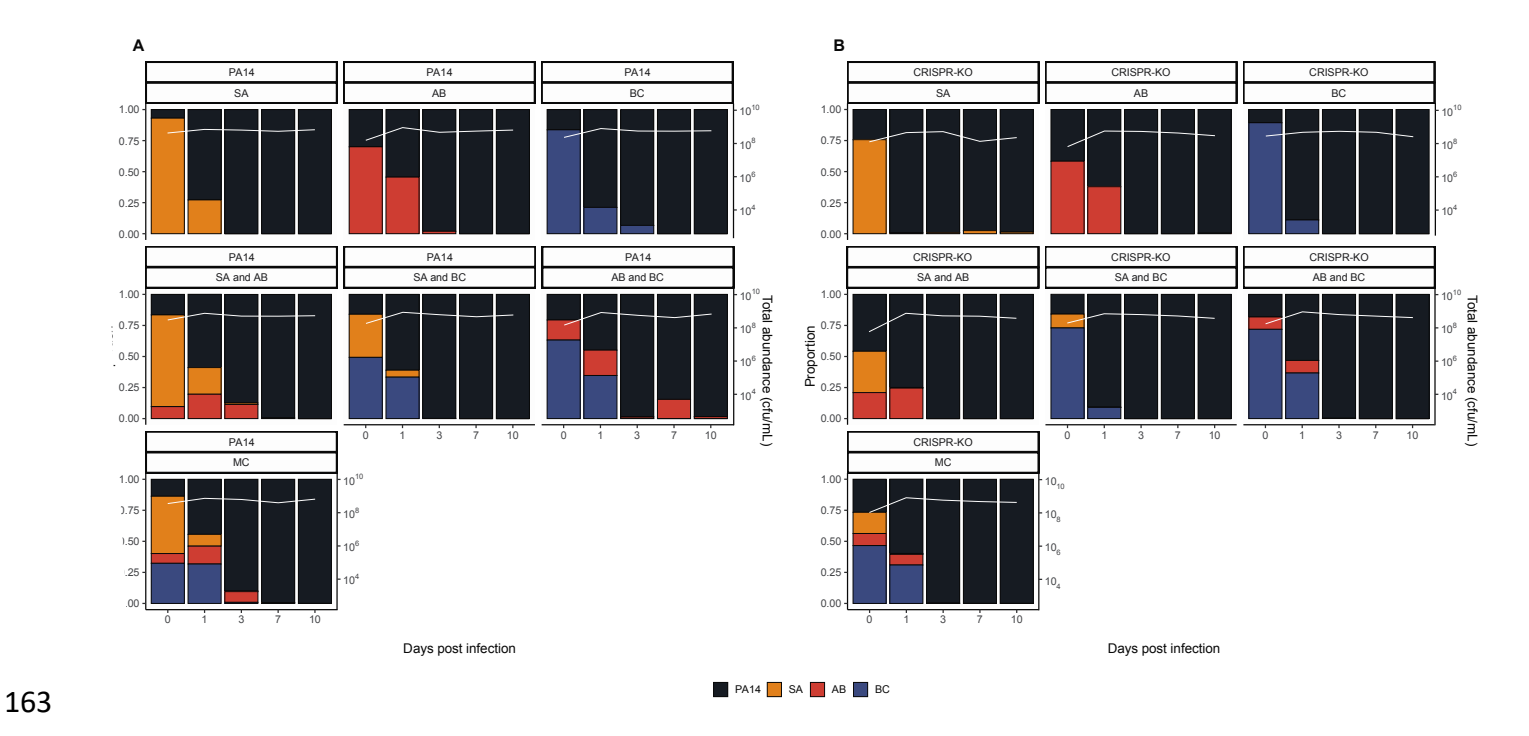


**Fig 2.** *Pseudomonas aeruginosa* becomes the dominant species in the absence of phage. Showing the community composition and bacterial densities in cfu/mL over time for the microbial communities in the absence of phage for the communities with either the **A** PA14 WT or **B** CRISPR-KO mutant. The community composition was estimated by qPCR at days 0, 1, 3, 7 and 10 of the experiment. The coloured bars represent the relative abundance of each species (left y axis), while the white line represents total abundance in cfu/mL (right y axis). Each panel represents average composition across six replicates for each treatment over time. PA14 = *P. aeruginosa*, SA = *S. aureus*, AB = *A. baumannii*, BC = *B. cenocepacia*, MC = microbial community. For individual replicates of species abundance, see Fig. S3.

While the microbial community dynamics were relatively similar for the WT and CRISPR-KO strains, some significant differences were observed. For example, the densities of the CRISPR-KO strain were slightly lower in the presence compared to the absence of *S. aureus* on its own (Fig 2, linear model: t = 2.048, p = 0.0413; overall model fit; adjusted  $R^2 = 0.21$ ,  $F_{36,345} = 3.77$ ,  $p < 6.03 \times 10^{-11}$ ). Moreover, *S. aureus* and *A. baumannii* reached higher densities in the presence of the PA14 WT compared to the CRISPR-KO strain, particularly at the earlier timepoints (Fig 2). In contrast to this, densities of *B. cenocepacia* over time were similar in the presence of both *P. aeruginosa* genotypes (Fig 2). Regardless these minor differences, *P. aeruginosa* consistently and readily outcompeted the other community members in the absence of phage, with all three being extinct or close to extinction by day 10 (Fig 2). For visualisation purposes, the data from Figure 2 is also presented as an ordination plot (Fig S2).

## Phage affects microbial community dynamics

Whereas *P. aeruginosa* dominated in the absence of phage, we hypothesised this would change once a PA14 targeting phage (DMS3vir) was introduced, largely by a virulent phage reducing the susceptible host population, facilitating expansion of other species through competitive release [14,52–55]. As expected, phage DMS3vir initially reached high titres due to replication on sensitive *P. aeruginosa* hosts, followed by a rapid decline in phage densities due to the evolution of phage resistance, regardless of whether the host had a functional CRISPR-Cas system or not (Fig 3C). Crucially however, the presence of phage caused microbial communities to no longer be dominated by *P. aeruginosa*, as when compared to the no phage treatments, very few to none of the

experimental repeats had one or more bacterial species go extinct, with *A. baumannii* reaching particularly high abundance (Figs 3A, 3B and S5). It is here worth noting that while *B. cenocepacia* is not visible at later timepoints in the compositional plot due to low relative abundance of <0.1 (Fig 3A and 3B), we consistently observed persistence of *B. cenocepacia* at an average of  $\sim 10^4$  cfu/mL across all treatments (see Fig S4). For visualisation purposes, the data from Figure 3 is also presented as an ordination plot (Fig S5).

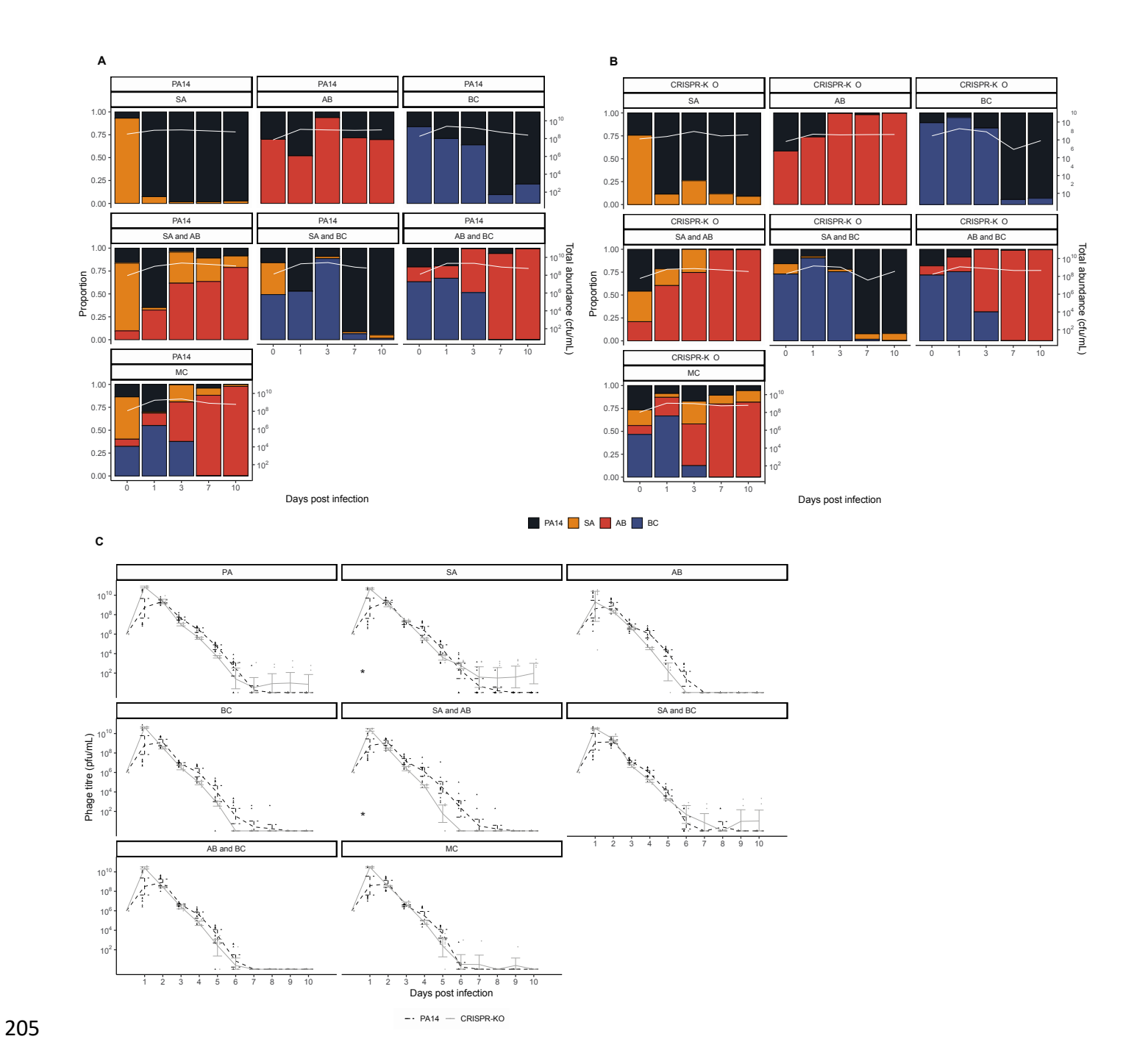


**Fig 3.** Phage allows for the maintenance of all microbial community members, with **A.** baumannii becoming the new dominant species. Showing the community composition and bacterial densities in cfu/mL over time for the microbial communities in the absence of phage for the communities with either the **A** PA14 WT or **B** CRISPR-KO mutant. For **A** and **B**, the community composition was estimated by qPCR at days 0, 1,

3, 7 and 10 of the experiment. The coloured bars represent the relative abundance of each species (left y axis), while the white line represents total abundance in cfu/mL (right y axis). Each panel represents average composition across six replicates for each treatment over time. PA14 = *P. aeruginosa*, SA = *S. aureus*, AB = *A. baumannii*, BC = *B. cenocepacia*, MC = Microbial community. For individual replicates of species abundance, see Fig. S4. **C** Phage titres for phage DMS3vir over time across all experimental treatments (PA = *P. aeruginosa*, SA = *S. aureus*, AB = *A. baumannii*, BC = *B. cenocepacia*, MC = microbial community), infecting either the PA14 WT or the CRISPR-KO strain as indicated by line type. Each data point represents a replicate, with lines following the mean and the error bars denoting 95% CI. Asterisks indicate a significant overall difference in phage density between the PA14 WT (n = 12 per timepoint) or CRISPR-KO clone (n = 6 per timepoint) (effect of *P. aeruginosa* clone; linear model: \* p < 0.05).

Interestingly, the PA14 WT generally reached greater relative abundance than the CRISPR-KO strain when in the presence of A. baumannii, consistently doing so early in the experiment when phage remained in the population (Figs 3A, 3B and S2). This was in concordance with P. aeruginosa evolving higher levels of CRISPR-based immunity against phage DMS3vir in treatments including A. baumannii due to the increased fitness cost of surface modification (Fig 4 and [15]): At 3 days post infection, there was a significant effect of all treatments on the proportion of CRISPR-based resistance that had evolved compared to the PA14 monoculture, but this effect was strongest for treatments that contained A. baumannii. At timepoint 10 we only found an increased proportion of P. aeruginosa clones immune through CRISPR-Cas when the treatment included A. baumannii (GLM; A. baumannii; t = 2.637, p = 0.01; S. aureus and A. baumannii, t = 2.283, p = 0.025; A. baumannii and B. cenocepacia, t = 2.689, p = 0.0087; polyculture, t = 2.141, p = 0.035). Overall, however, it was evident that mutation of the Type IV pilus became the dominant resistance mechanism even if P. aeruginosa has a functional CRISPR system (Fig 4), which might in part be why *P. aeruginosa* did not recover in the microbial community post phage exposure due to the associated fitness costs[15].

225

226

227

228

229

230

231

232

233

234

235

236

237

238

239

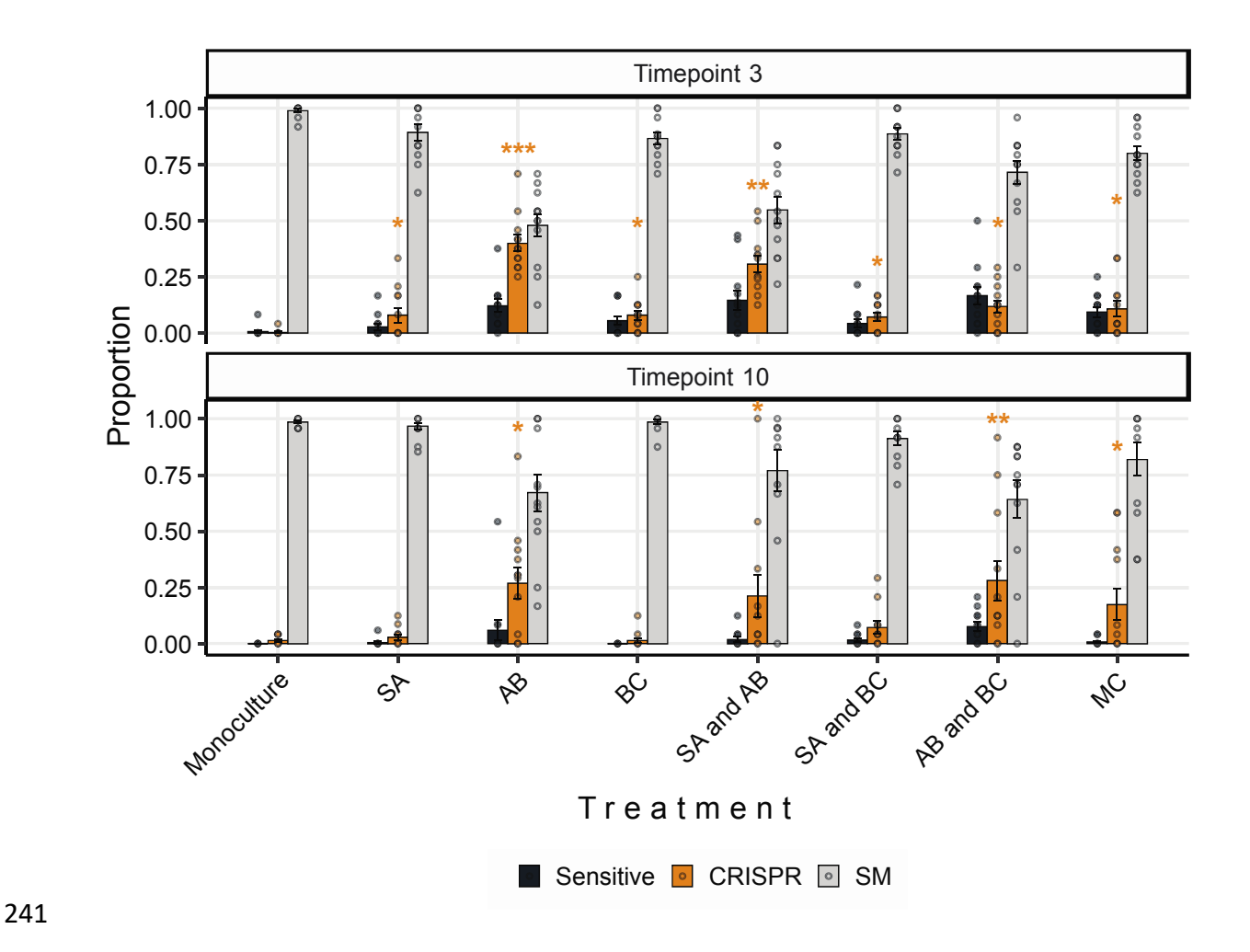


**Fig 4.** Interspecific competition affects the proportion of evolved CRISPR-based phage resistance. Proportion of *P. aeruginosa* PA14 WT at timepoints 3 and 10 that evolved phage-resistance either through surface modification (SM) or CRISPR immunity, or which remained sensitive to phage DMS3vir when grown in monoculture or different polycultures (SA = S. aureus, AB = A. baumannii, BC = B. cenocepacia). Data are mean  $\pm$  SE. Asterisks indicate a significant difference in proportion of CRISPR immunity evolved when compared to the PA14 monoculture within each timepoint (n = 12 per treatment) (generalised linear model, quasibinomial: \* p < 0.05, \*\* p < 0.01, \*\*\* p < 0.001).

# The type of evolved phage resistance does not have a knock-

# on effect on microbial community dynamics

Phage DMS3vir targets *P. aeruginosa's* Type IV pilus (T4P), an important virulence factor [56]. We have previously shown that the evolution of phage resistance by mutation of the pilus is associated with large fitness trade-offs in the same microbial community as used in this study, whereas evolution of CRISPR-based immunity is not associated with any detectable trade-offs [15]. We therefore predicted that the ability to evolve phage resistance through CRISPR-Cas would also have knock-on effects for the microbial community dynamics. However, measurement of the abundance of the competitors revealed that these were overall largely unaffected by the presence of a functional CRISPR-Cas immune system in P. aeruginosa with the exception of S. aureus: In the presence of the *P. aeruginosa* WT strain, *S. aureus* densities were significantly lower in two of the microbial communities compared to the same co-culture experiments with the CRISPR-KO strain (Figs 3 and S4, Effect of *P. aeruginosa* clone on *S. aureus* abundance, linear model: Treatment S. aureus; t = -2.363, p = 0.0216, adjusted  $R^2 = 0.2659$ ,  $F_{14,57} = 0.0216$ 2.837, p = 0.002786; Treatment S. aureus and A. baumannii; t = -2.043, p = 0.0457, adjusted  $R^2 = 0.3867$ ,  $F_{14,57} = 4.198$ ,  $p = 5.3 \times 10^{-5}$ ).

267

268

269

270

271

250

251

252

253

254

255

256

257

258

259

260

261

262

263

264

265

266

# A *P. aeruginosa* targeting phage results in the competitive release of *A. baumannii* and general diversity maintenance

We hypothesised that the effect of phage on microbial community structure could largely be explained by the competitive release (increase in absolute abundance, following removal of competitor) of *A. baumannii*, which then takes over to become the dominant species [57]. To assess this, we examined the fold change difference for the final abundance of all three community members in the presence versus absence of phage (Fig 5). Crucially, this revealed a strong increase in *A. baumannii* density in the presence of a phage, supporting the idea that it becomes the dominant and determinant community member when *P. aeruginosa* is inhibited by phage (Fig 3). By contrast, when phage was added, *S. aureus* only experienced a clear fold change increase if it was co-cultured with the CRISPR-KO strain and an additional competitor species. *B. cenocepacia* meanwhile seemed to be the species with the least benefit of phage, but still with a small fold change increase for some treatments (Fig 5).

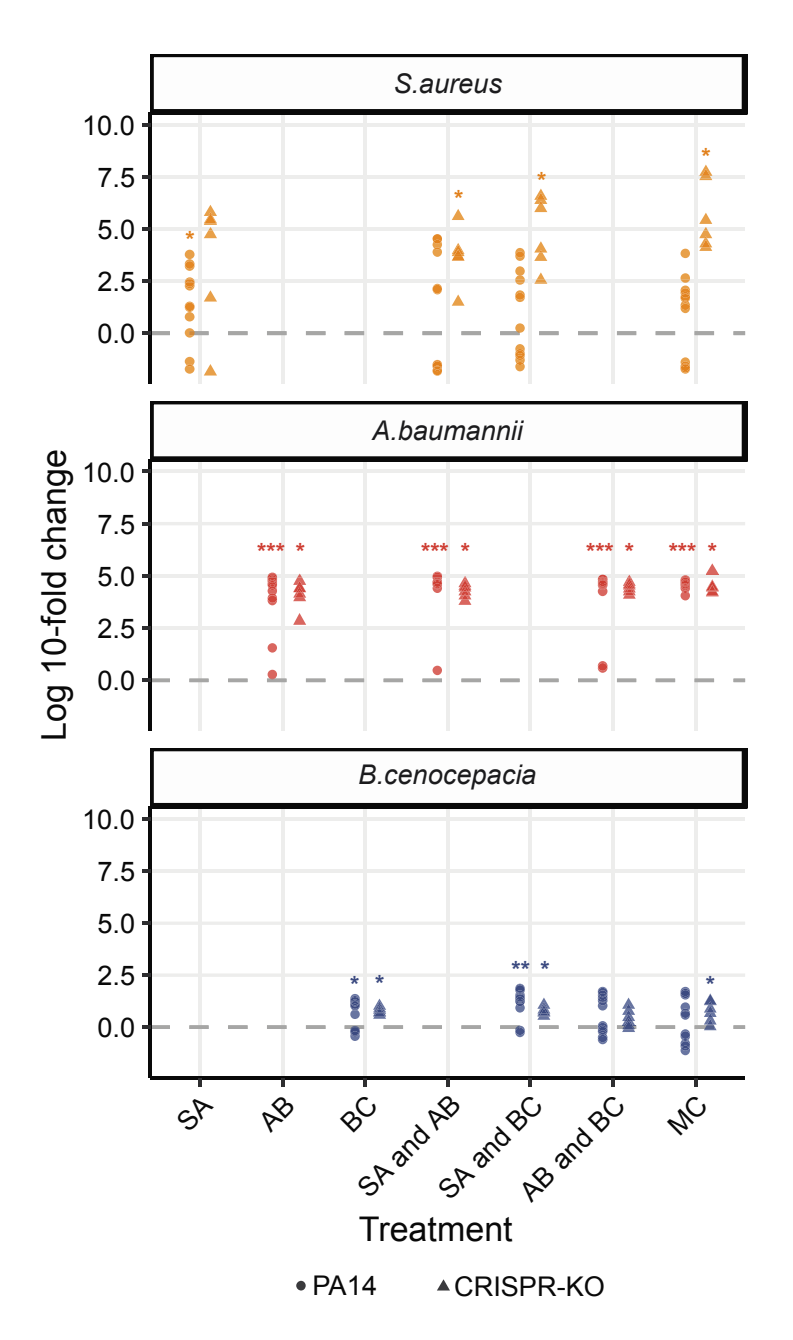


Fig 5. Fold change between no phage and phage treatments at the end of the experiment. The fold change difference of the individual community species not targeted by phage when comparing absolute densities in the presence of phage to the absence at the final experimental timepoint. Asterisks indicate higher final absolute density in the presence versus absence of phage (Wilcoxon signed rank exact test: \* p < 0.05, \*\* p < 0.01, \*\*\* p < 0.001).

The substantial fold increase in *A. baumannii* given the presence of phage (Fig 5) reflects a sustained divergence in the trajectory of *A. baumannii* in the phage treatments, despite the attenuation of phage titre by day 7 (Fig 3C). We hypothesised that the lack of *P. aeruginosa* rebound after phage clearance was due to a frequency-dependent shift in competitive dominance. To test this hypothesis, we competed ancestral *A. baumannii*, *S. aureus* and *B. cenocepacia* against increasingly rare *P. aeruginosa* challenge, and found no barrier to *P. aeruginosa* invasion in pairwise experiments, down to a frequency of 1 in 10,000 cells (Fig 6). This result suggests that the failure of *P. aeruginosa* to return to dominance following phage clearance is due to more complex community-mediated interactions.

Additionally, we tested if it was *A. baumannii* that could have gained an advantage through natural selection when competing against *P. aeruginosa* over time, with phage allowing *A. baumannii* to better adapt to the environment and explain the inability of PA14 to reinvade. Yet our data demonstrated that there was no difference in competitive performance of evolved *A. baumannii* relative to its ancestral strain, and both the ancestor and the evolved clonal populations of *A. baumannii* were outcompeted by the PA14 wild-type (Fig. 7).

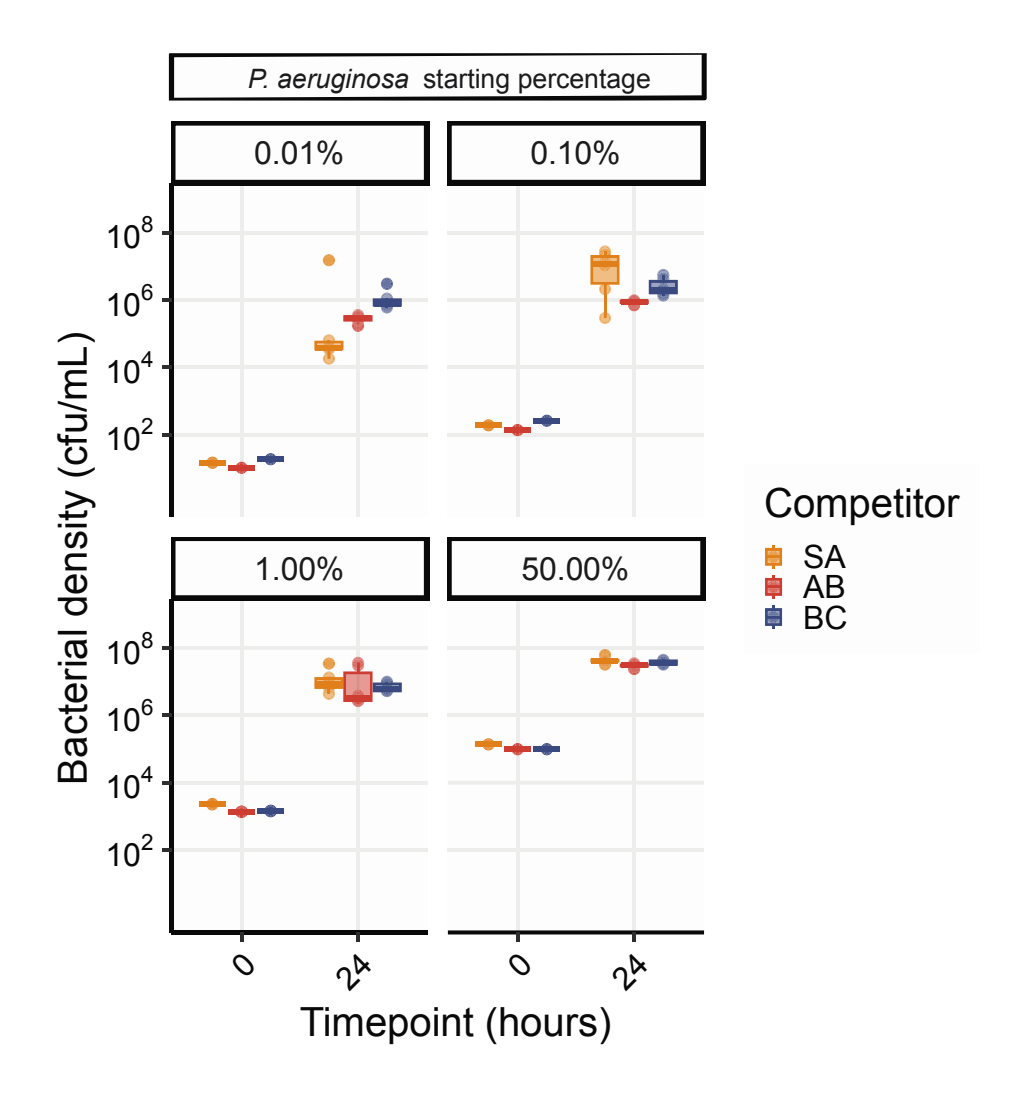


Fig 6. *P. aeruginosa* can invade from low initial frequency against all community members.

Showing *P. aeruginosa* density in cfu/mL from competition experiments between PA14 wild-type with variable starting densities against either *S. aureus* (SA), *A. baumannii* (AB) or *B. cenocepacia* (BC). The species densities were estimated by qPCR at time-point 0 and 24 h post co-culture. Box plots show the median, 25th and 75th percentile, and the interquartile range. Raw values from each biological replicate are shown as points (n= 6 per pairwise competition).

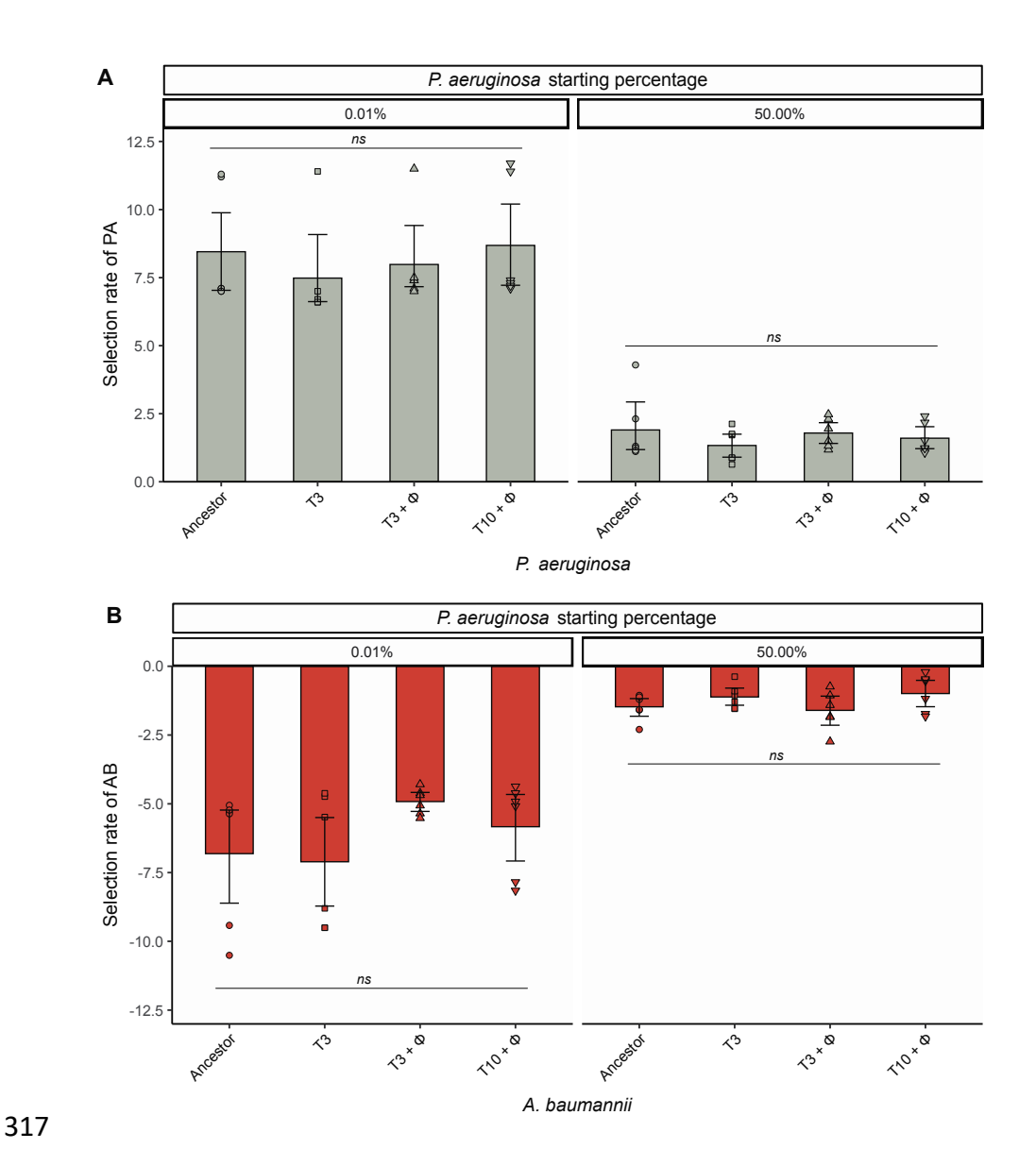


Fig 7 | *P. aeruginosa* and *A. baumannii* fitness levels remained unaffected during the 10-day evolution experiment. A Selection rate [58,59] of evolved and ancestral PA14 (PA = *P. aeruginosa*) in pairwise competition with the *A. baumannii* wild-type. **B** Selection rate of evolved and ancestral *A. baumannii* (AB = *A. baumannii*) in pairwise competition with wild-type PA14. Ancestor represent wild-type strain; T3 and T3 +  $\varphi$  correspond to clones recovered at 3 days post co-culture from 10-day evolution experiment with PA14 and *A. baumannii* without or with DMS3vir phage, respectively;

T10 +  $\varphi$  represent competition with clones recovered at 10 days post co-culture with *A. baumannii* and phage DMS3vir. Selection rate is the difference of Malthusian growth parameters of PA14 or *A. baumannii* against competitor [58,59]. The line at zero indicates no difference in density change (i.e. both are equally fit). Data shown are the mean  $\pm$  95% CI and individual biological replicates are plotted as symbols (n = 6). ns = not significant, using one-way ANOVA test for multiple comparison.

To quantitatively assess changes in community diversity, we calculated Shannon diversity indexes for all experimental treatments. We hypothesised that the addition of phage not only results in competitive release of one other bacterium (Fig 5), but facilitates general maintenance of microbial diversity. Plotting these diversity scores over time shows that without phage there is a rapid loss of diversity over time, whereas community complexity persists in the presence of phage (Fig 8: ANOVA: PA14 WT effect of phage; F = 27.57,  $P = 2.3 \times 10^{-7}$ ; CRISPR-KO effect of phage; P = 89.19,  $P < 2.2 \times 10^{-16}$ ; Overall model fit for PA14 WT: adjusted P = 0.64, P = 0.6

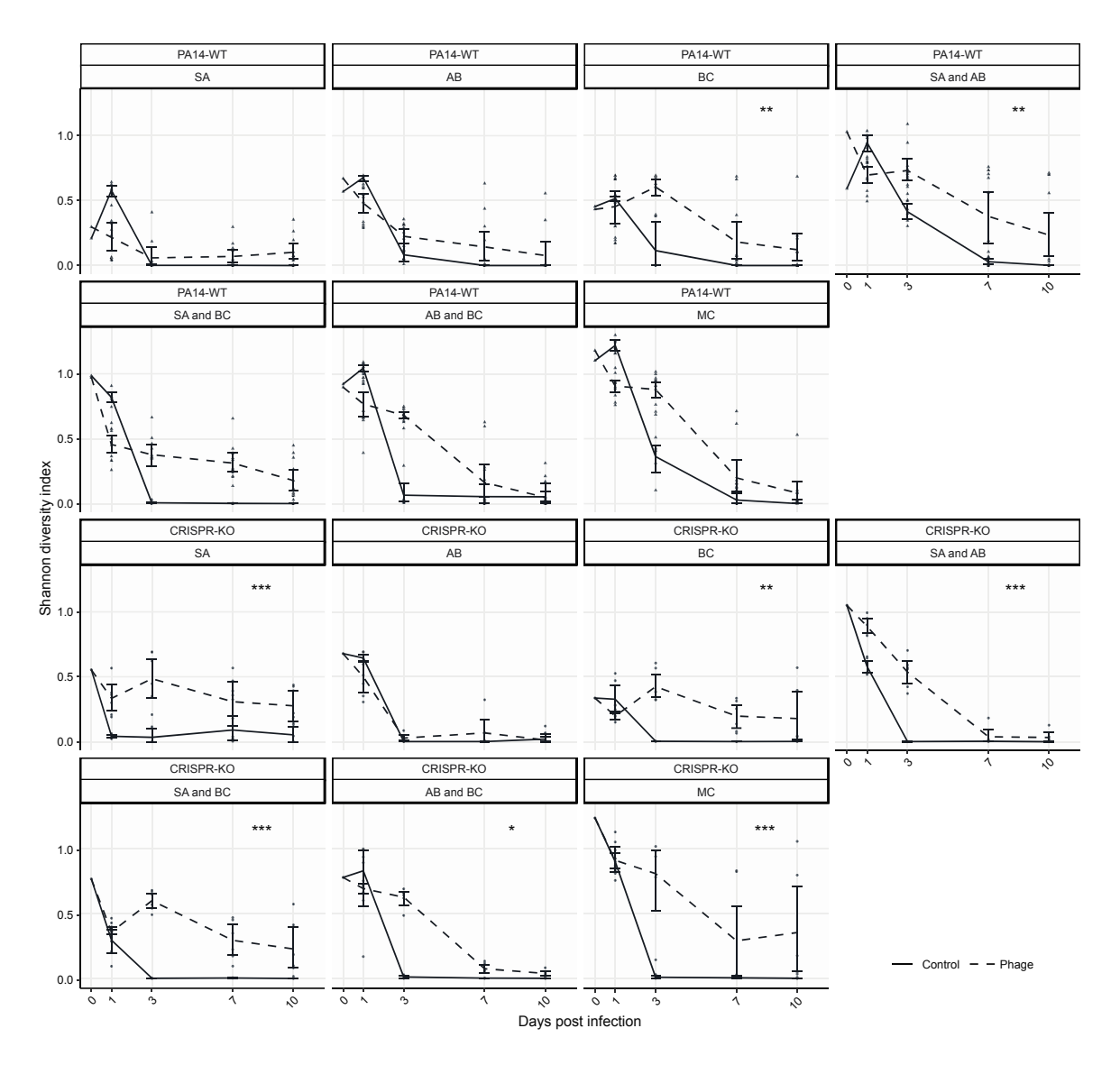


Fig 8. Shannon diversity over time illustrating the diversity maintaining effects of phage. The change in diversity over time, illustrated using Shannon diversity indexes, for both the PA14 WT and CRISPR-KO strains across all treatments (SA = S. aureus, AB = A. baumannii, BC = B. cenocepacia, MC = microbial community). Data are mean  $\pm$  95% CI, and asterisks indicate a significant difference over time in Shannon diversity between treatments with phage or no phage (n = 6 per timepoint for all expect the PA14 WT with phage treatments, where n = 12) (effect of P. aeruginosa clone; linear model with Tukey contrasts: \* p < 0.05, \*\* p < 0.01, \*\*\* p < 0.001).

355

356

357

358

359

360

361

362

363

364

365

366

367

368

369

Four species community dynamics are predictable from two and three species community data, in the absence of phage Mathematical modelling provides a platform to quantify ecological interactions that determine community level behaviours, as well as identify rules governing qualitative system behaviour [60–63]. However, a major challenge in synthetic community research is developing robust modelling frameworks that are capable of predicting community dynamics [64]. In a final set of analyses, we sought to parameterise and assess the predictive performance of generalized Lotka Volterra (gLV) competition equations, trained on just 2-species data or a combination of 2- and 3-species data. Our results showed that fitting gLV models with pairwise only datasets led to predictive failures when applied to 3or 4-species datasets (Fig S6), consistent with the presence of higher order interactions effects (when the effect of species A on species B is dependent on the presence of species C [65]). In contrast, fitting gLV models to 2- and 3-species data and using the resulting interaction terms to predict 4-species dynamics reasonably fit the data in the absence of phage (Fig 9; fitted model coefficients are in Fig. S8).

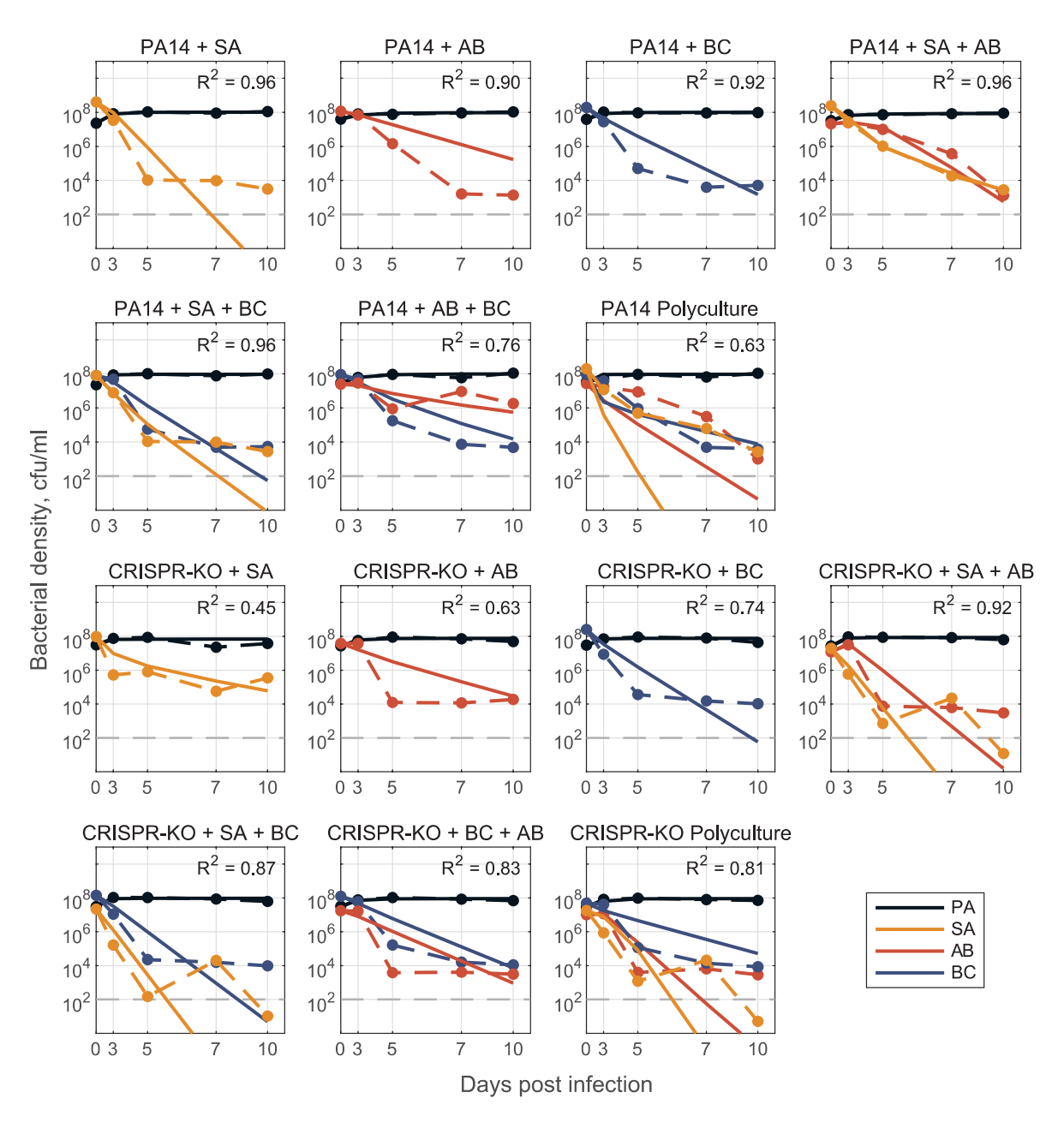


**Fig 9. Model for no phage data.** Model fit predictions for two-, three-, and full four species community dynamics (solid lines) compared to experimental data (dashed lines) (PA = P. aeruginosa, SA = S. aureus, AB = A. baumannii, BC = B. cenocepacia). Models of 2- and 3- species dynamics were parameterized via optimization with least-squares to fit to a system of ODEs (defined as a generalized Lotka-Volterra competition model with n species, where n=1,2,3,4). Only single species maximal growth rates ( $r_i$ 

for species i=1,...,n) were fixed from fitting mono-culture data, all interaction coefficients ( $\beta_{i,j}$  describing the inhibitory effect of species j on species i for all i,j=1,2 in the 2-species case, for all i,j=1,2,3 in the 3-species case) were open for fitting. We construct the full 4-species community interaction matrices (one for PA14—shown in Fig. S8—and one for CRISPR-KO) by averaging corresponding  $\beta_{i,j}$  interaction terms from the fit 2- and 3- species models (see Text S1), and use this matrix to simulate dynamics in the respective polyculture cases. See Methods and Text S1 for detailed description of mathematical modelling.

In the presence of phage (Fig 10), we again utilised the gLV framework where the impact of phage is implicit (quantified by how interaction coefficients change as compared to the no-phage case). The gLV model framework could adequately describe 2- and 3-species data, but the interaction coefficients did not generalise quantitatively to 4-species data – likely reflecting the structural limitation of a gLV competition model that does not explicitly capture phage predation dynamics. However, the model parameterised with 1-, 2- and 3-species data did capture a qualitative shift in ecological outcomes from sole *P. aeruginosa* survival to competitive release of *A. baumannii* and *S. aureus* when *P. aeruginosa* is targeted by phage (Fig S7).

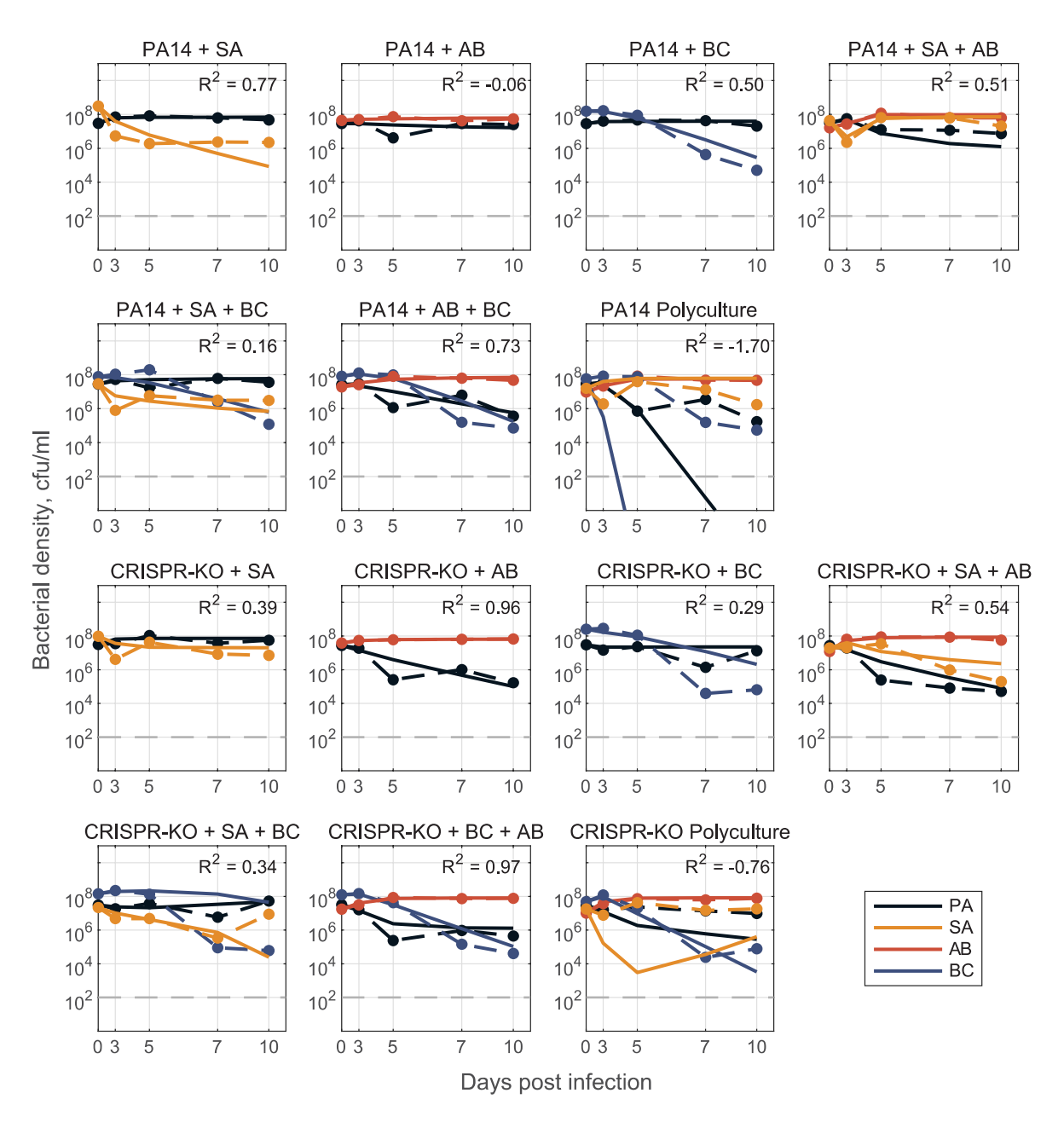


**Fig 10. Model for phage data.** Model fit predictions for two-, three-, and full four species community dynamics (solid lines) in the presence of phage compared to experimental data (dashed lines) (PA = P. aeruginosa, SA = S. aureus, AB = A. baumannii, BC = B. cenocepacia). Here, models were parameterized via optimization with least-squares to fit a system of ODEs (defined as a generalized Lotka-Volterra competition model with n species, where n=1,2,3,4), where we don't explicitly track the

phage population dynamics. Instead, we assume that the phage acts as some external perturbation that leads to changes in the interactions between community members ( $\beta_{i,j}$  values differ from values in Fig 9). Only single species maximal growth rates were fixed from fitting mono-culture data ( $r_i$  for species i=1,...,n), all interaction coefficients were open for parameterizing 2- and 3- species models ( $\beta_{i,j}$  describing the inhibitory effect of species j on species i for all i,j=1,2 for the 2-species case, for all i,j=1,2,3 for the 3-species case). We then construct the full 4-species community interaction matrices (one for PA14 and one for CRISPR-KO) by averaging corresponding  $\beta_{i,j}$  interaction terms from the fit 3- species models (treatments: PA+AB+SA, PA+BC+SA, PA+AB+BC with phage), and use this matrix to simulate dynamics in the respective polyculture cases. See Methods and Text S1 for detailed description of mathematical modelling.

## **Discussion**

The advent of deep sequencing has dramatically increased our knowledge of the composition and functioning of microbiomes both in and around us. The role of microbial communities in human health has consequentially received increasing attention, with research focusing on how changes in microbiome composition over time may affect human health and define patient outcomes (reviewed in [66]). In addition, an increasing number of correlational studies find associations between virome composition and the health status of their host [23,67–70], likely mediated by changes in the microbiome that could be either cause or effect. A deeper understanding of the impact of phages on microbiomes is likely to help to infer causal relationships between viromes and human health, and to design optimal therapeutic phage interventions (phage therapy).

426

427

428

429

430

431

432

433

434

435

436

437

438

439

440

441

Here, we expanded on our previous work on how interspecific competition can shape the evolution of phage resistance in a focal species (P. aeruginosa)[15], to study how the interaction between phage and bacterial immune mechanisms affects the broader microbial community dynamics. We found that whereas P. aeruginosa dominated in the absence of a phage, the presence of phage resulted in microbial diversity maintenance and A. baumannii becoming the dominant species (Figs 3 and 5). Interestingly, the competitive release of A. baumannii occurred in all treatments and was virtually independent of whether *P. aeruginosa* had a functional CRISPR-Cas immune system or not. This showed that the amplification of the fitness cost of *P. aeruginosa* receptor mutation in the presence of competitor species [15] has limited impact on the overall community dynamics. Overall, our experimental data align with the notion of phages having the potential to increase diversity and microbiome stability [27,71,72], and support the idea that phages can be useful in the designing of synthetic microbial communities [73]. Surprisingly, our data do not support the hypothesis that bacterial adaptive immune systems play an important role in phage-mediated microbial community structuring under the experimental conditions tested here.

442

443

444

445

446

447

Our mathematical analyses focused on the ability of generalised Lotka-Volterra (gLV) models to predict community dynamics. While our analyses showed reasonable predictive success when incorporating 3-species data, we note that our analyses pose two distinct questions: (1) how can we provide more accurate predictions? (2) what general lessons can we draw from our model analyses?

449

450

451

452

453

454

455

456

457

458

459

460

461

462

463

464

In agreement with a growing number of gLV-based analyses, we found that a simple 'bottom up' model fitting approach (fitting single species growth, then all pairwise interactions, then predicting larger system behaviour [14]) performed poorly, indicating the presence of significant higher order interactions [65,74,75]. Consistent with this conclusion, we found that allowing pairwise interactions to vary (contingent on the presence of a third species) produced both qualitative and quantitative improvements in predicting community dynamics (Figs 9 and 10). In the presence of phage, our model successfully predicted the qualitative result of A. baumannii competitive release, but failed to quantitatively replicate observed community dynamics (Fig 10). This quantitative failure suggests that our underlying gLV model structure (the dominant framework in microbiome modelling studies [61,71,76]) excludes critical components, such as higher order and/or heterogeneous (in time or space) interactions as well as the explicit predatory effect of phage on P. aeruginosa (also likely time and spatially dependent). Additionally, it emphasises an ongoing need in microbiome modelling to evaluate functional forms that can efficiently - with respect to parameter number - and accurately capture the complexities of community dynamics.

465

466

467

468

469

470

Our parameterised models are tuned to the data generated by our specific 4-species community, which raises the question of 'can we learn more general lessons from our model?' If we simplify our analysis to a 2-species context (focal pathogen, subject to phage, plus a second, non-focal species), we can translate recent analyses on the impact of (antibiotic) perturbations in a two species context [55]. This approach delivers a couple

of general messages. First, we can provide a general mathematical definition of 'competitive release' mediated by phage predation (see Text S1) highlighting the importance of both demographic and species interaction parameters. Second, we can underline that phage control of a focal pathogen presents secondary ecological problems, if the pathogen is competing with other pathogens that are not targeted by the phage. In this scenario, phage therapy (or other 'narrow spectrum' treatment) can lead to competitive release of previously rare pathogens, as seen in our experimental data showing the replacement of *P. aeruginosa* by *A. baumannii*, following phage treatment. These results imply that 'narrow spectrum' anti-microbials, such as phages, may not always be the best option when multiple pathogen species are competing within a single polymicrobial infection. One counter-intuitive suggestion, grounded in the idea of 'beneficial resistance' [55], is to co-administer probiotic competitors that are resistant to the treatment (i.e. phage or antibiotic resistant) and can therefore continue to exert ecological suppression on the focal pathogen during the course of treatment, while presenting minimal direct risk of disease. Alternatively, one could apply phage cocktails that target not just the dominant pathogen, but also other co-existing bacterial pathogens, to pre-emptively prevent their invasion.

488

489

490

491

492

493

471

472

473

474

475

476

477

478

479

480

481

482

483

484

485

486

487

## **Materials and Methods**

# **Bacteria and phages**

The bacteria *P. aeruginosa* UCBPP-PA14 strain marked with streptomycin resistance, the PA14 *csy3::LacZ* strain (CRISPR-KO), and phages DMS3vir and DMS3vir+acrF1 were used throughout this study and have all been previously described [77,78]. The

microbial community consisted of *S. aureus* strain 13 S44 S9 and *A. baumannii* clinical isolate FZ21 which were isolated at Queen Astrid Military Hospital, Brussels, Belgium, while *B. cenocepacia* J2315 was originally isolated from a person with cystic fibrosis in the UK in 1989 and was provided by Queen Astrid Military Hospital, Brussels, Belgium.

498

499

500

501

502

503

504

505

506

507

508

509

510

511

512

513

514

515

516

497

494

495

496

### **Evolution experiment**

The evolution experiment was performed by inoculating 60 µl from overnight cultures, that were grown for 24 hours, into glass microcosms containing 6 ml fresh LB medium (60 µl of culture containing ca. 10<sup>6</sup> cfu). All polyculture mixes were prepared so that P. aeruginosa made up approximately 25% of the total inoculation volume (15 μl of 60 μl), with the rest being made up of one or equal amounts of the microbial community bacteria. In all monoculture controls, P. aeruginosa was diluted in LB medium to adjust starting densities for consistency across all treatments (n = 6 per treatment, unless indicated otherwise). Phage DMS3vir was added at 10<sup>6</sup> pfu. prior to inoculation. The experiment ran for ten days, with transfers of 1:100 into fresh LB medium being done every 24 hours. Throughout the experiment, the bacterial mixtures were grown at 37°C and shaking at 180 r.p.m. Phage titres were monitored daily, and plague counts were determined using chloroform-treated lysate dilutions which were spotted onto lawns of P. aeruginosa csy::LacZ. To determine which mechanism of phage-resistance had evolved, 24 randomly selected clones per treatment replica from timepoints 3 and 10 were analysed using methods as detailed in Westra et al. 2015 [78]: In brief, whether and how bacteria evolved phage resistance was done by doing cross-streak assays on phages DMS3vir and DMS3vir+acrF1, as well as PCR, on 24 random clones from each replicate

experiment for both the PA14 and CRISPR-KO treatments. Further sequencing of receptor mutants was not done due to a clear morphological difference associated with modifications to the Type IV pilus, as well as mutants with the same evolved morphology from similar experiments having previously been sequenced [79].

### **DNA extraction and qPCR**

Bacterial densities, for both PA14 strains and the other individual microbial community bacteria, were determined using DNA extractions followed by qPCR analyses. DNA extractions were done using the DNeasy UltraClean Microbial Kit (Qiagen), following instructions from the manufacturer, but with an additional pre-extraction step where samples were treated with 15 µl lysostaphin (Sigma) at 0.1 mg ml<sup>-1</sup> as previously described [15] to ensure lysis of *S. aureus*. The qPCR primers for *P. aeruginosa*, *A. baumannii*, and *B. cenocepacia* were the same as in Alseth *et al.* [15], whereas the *S. aureus* primers used are previously described [80]. All reactions were done in triplicates, using Brilliant SYBR Green reagents (Agilent) and the Applied Biosystems QuantStudio 7 Flex Real-Time PCR system. For reaction mixture and details on PCR programme, see ref. [15]. Bacterial cfu/mL were calculated from the quantities obtained by the standard curve method, adjusting for gene copy number (4, 1, 6, and 6, for *P. aeruginosa*, *S. aureus*, *A. baumannii*, and *B. cenocepacia* respectively).

### **Competition experiments**

All strains were grown overnight at 37°C with agitation in 30 ml glass universals containing 6 ml of LB medium. For pairwise competition assays, bacteria from overnight cultures

were mixed thoroughly at different starting densities of PA14 (i.e., for 50% starting density of P. aeruginosa we would mix 30  $\mu$ l of PA14 + 30  $\mu$ l of competitor strain) and a total of 60  $\mu$ l inoculated into 6 ml of LB (each treatment contained n = 6 biological replicates). Bacteria were grown for 24 hours in a shaking incubator at 180 r.p.m at 37°C. Samples of 500  $\mu$ l were taken at 0 and 24 hours post competition and mixed with equal volume of 60% glycerol and stored at -70°C until further DNA extraction and qPCR analysis to quantify species densities.

To assess the competitive fitness of evolved clones from the 10-day evolution experiment with and without phage DMS3vir we performed time-shift competition assays. Briefly,  $500\mu\text{L}$  of glycerol stock from each microcosm (n=6 per treatment) were plated onto selective media (Cetrimide agar (Invitrogen) for PA14 selection and LB agar supplemented with  $50~\mu\text{g/mL}$  of gentamicin to select for *A. baumannii*) and 6 randomly selected colonies from each replicate of indicated treatment/timepoint were pooled and inoculated overnight in 6 mL of LB medium at  $37^{\circ}\text{C}$  with agitation (n=6 per treatment, unless indicated otherwise). In parallel, 6 colonies from the ancestral strains were pooled and subject to the same overnight growth conditions. After 24h of growth, competition assay and sample treatments were performed as described above.

To determine the competitive performance of the focal species relative to competitor strain we used the selection rate (r), defined as the difference in Malthusian parameters as follows:  $r = (\ln[\text{density strain A at day } t/\text{density strain A at } t-1] - \ln[\text{density strain B at } t-1])/\text{day})$  [58,59]. The data used for these calculations were the

bacterial quantities (cfu/mL) as estimated by qPCR as explained above, with two technical replicates per assay.

565

566

567

568

569

570

571

572

573

574

575

576

577

578

579

580

581

582

583

563

564

### **Mathematical modelling**

Models were parameterized via optimization with least-squares regression to fit the generalized Lotka-Volterra competition model,  $\frac{dN_i}{dt} = r_i N_i - \sum_{j=1}^n \beta_{ij} N_i N_j$ , where  $N_i(t)$  is the density of the *i*th species,  $r_i$  is the respective single species maximal growth rate,  $\beta_{ij}$ describes the per capita effect of species i on species i, and n is the total number of species. We take a 'bottom up' approach [81] to determine the interaction coefficients  $\beta_{i,j}$ . In all cases, we determine single species maximal growth rates  $r_i$  from mono-culture time series data and fix them for 2-, 3-, and 4-species model parameterization. Initially, we fit pairwise interaction coefficients for all possible 2-species co-cultures and from here, construct an interaction matrix to predict the dynamics for the 3- and 4- species communities (Fig S6). This is done for both PA14 and CRISPR-KO strains, with and without phage, where phage effects are implicitly represented by changes in interaction parameters between the models with and without phage. To improve results, we additionally fit pairwise interaction parameters  $\beta_{i,j}$  using 3-species experimental data where all interaction parameters are open (only growth rates fixed). Using either the resulting interaction terms or averaging these coefficients with the 2-species coefficients (in PA14 no phage case, Text S1), we are again able to construct an interaction matrix to predict 4-species community dynamics (Fig 9 and 10).

See Text S1 for further description of above model parameterization methods, simulation methods (Fig S7), and mathematical analysis of phage dependent competitive release. All modelling and analysis was done using Matlab 2021b and the code is publicly available at: <a href="https://github.com/GaTechBrownLab/phage-community-dynamics.git">https://github.com/GaTechBrownLab/phage-community-dynamics.git</a>.

589

590

591

592

593

594

595

596

597

598

599

600

601

602

603

604

605

606

607

588

585

586

587

## Statistical analyses

Analysis of the effects of the various species compositions on *P. aeruginosa* densities in the absence (Fig 2) or presence (Fig 3) of phage were done using a generalised linear model (GLM) approach, with log10 cfu/mL set as the response variable. The explanatory variables used in the analyses were type of PA14 clone (PA14 WT or CRISPR-KO), treatment, timepoint, replica, and experimental repeat to account for potential pseudoreplication. To explore the impact of interspecific competition on the evolution of phage resistance at timepoints 3 and 10 (Fig 4), we used a quasibinomial GLM where the proportion of evolved CRISPR-based phage resistance was the response variable, and treatment, replica, and experimental repeat were the explanatory variables. The analyses of fold-changes to assess competitive release by comparing absolute density differences of the individual community members in the absence v presence of phage (Fig 5; S. aureus, A. baumannii, and B. cenocepacia) was done through Wilcox signed rank exact tests. A non-parametric test was chosen after performing a Shapiro-Wilk test for normality. Next, the diversity maintaining effects were examined through assessing the effect of phage DMS3vir on Shannon Diversity index scores over time (Fig 8). This was done

through a linear model where the Shannon Diversity index score (H) was the response variable, and treatment, timepoint, the presence of phage, PA14 clone (PA14WT and CRISPR-KO), experimental repeat, and replica were the explanatory variables. Shannon Diversity (H), was calculated as H =  $-\Sigma p_i * ln(p_i)$ , where  $\Sigma$  is the sum and  $p_i$  is the proportion of the entire community made up of species i.

For the competition assay (Fig 6 and Fig 7), Graphpad Prism9 software (San Diego, CA) was used for statistical analysis. We used one-way ANOVA with Tukey post hoc testing for multiple comparisons, in which, p < 0.05 was considered statistically significant. Throughout the paper, pairwise comparisons were done using the Emmeans package [82], and model fits were assessed using Chi-squared tests and by comparing Akaike information criterion (AIC) values, as well as plotting residuals and probability distributions using histograms and quantile-quantile plots (Q-Q plots) respectively. All statistical analyses were done using R version 4.3.0. [83], its built-in methods, and the Tidyverse

## **Acknowledgements**

This work was supported by a grant from the ERC (ERC-STG-2016-714478 - EVOIMMECH), a Biotechnology and Biological Sciences Research Council (BBSRC) sLoLa grant BB/X003051/1, awarded to E.R.W, a NHI grant (NIH 5R21AI156817-02) awarded to S.P.B, and an NSF/BBSRC-National Science Foundation grant (NSF 2321502), awarded to S.P.B., R.A.K & E.R.W.

package version 2.0.0 [84]. All data is available at: 10.6084/m9.figshare.24187284.

## **Competing Interests**

E.R.W. is inventor on patent GB2303034.9.

632

633

## References

- 1. Byrd AL, Belkaid Y, Segre JA. The human skin microbiome. Nat Rev Microbiol. 2018;16: 143–155. doi:10.1038/nrmicro.2017.157
- Thursby E, Juge N. Introduction to the human gut microbiota. Biochem J. 2017;474:
   1823–1836. doi:10.1042/BCJ20160510
- 3. Pearl Mizrahi S, Goyal A, Gore J. Community interactions drive the evolution of antibiotic tolerance in bacteria. Proc Natl Acad Sci. 2023;120: e2209043119. doi:10.1073/pnas.2209043119
- 4. Manichanh C, Borruel N, Casellas F, Guarner F. The gut microbiota in IBD. Nat Rev
   Gastroenterol Hepatol. 2012;9: 599–608. doi:10.1038/nrgastro.2012.152
- 5. Freitas AC, Chaban B, Bocking A, Rocco M, Yang S, Hill JE, et al. The vaginal microbiome of pregnant women is less rich and diverse, with lower prevalence of Mollicutes, compared to non-pregnant women. Sci Rep. 2017;7: 9212. doi:10.1038/s41598-017-07790-9
- 6. Lloyd-Price J, Mahurkar A, Rahnavard G, Crabtree J, Orvis J, Hall AB, et al. Strains, functions and dynamics in the expanded Human Microbiome Project. Nature. 2017;550: 61–66. doi:10.1038/nature23889
- 7. Glassner KL, Abraham BP, Quigley EMM. The microbiome and inflammatory bowel disease. J Allergy Clin Immunol. 2020;145: 16–27. doi:10.1016/j.jaci.2019.11.003
- 8. Azimi S, Lewin GR, Whiteley M. The biogeography of infection revisited. Nat Rev Microbiol. 2022;20: 579–592. doi:10.1038/s41579-022-00683-3
- Scher JU, Sczesnak A, Longman RS, Segata N, Ubeda C, Bielski C, et al.
   Expansion of intestinal Prevotella copri correlates with enhanced susceptibility to
   arthritis. Mathis D, editor. eLife. 2013;2: e01202. doi:10.7554/eLife.01202
- Lam V, Su J, Hsu A, Gross GJ, Salzman NH, Baker JE. Intestinal Microbial
   Metabolites Are Linked to Severity of Myocardial Infarction in Rats. PloS One.
   2016;11: e0160840. doi:10.1371/journal.pone.0160840
- Livanos AE, Greiner TU, Vangay P, Pathmasiri W, Stewart D, McRitchie S, et al.
   Antibiotic-mediated gut microbiome perturbation accelerates development of type 1
   diabetes in mice. Nat Microbiol. 2016;1: 16140. doi:10.1038/nmicrobiol.2016.140
- 12. Surana NK, Kasper DL. Moving beyond microbiome-wide associations to causal microbe identification. Nature. 2017;552: 244–247. doi:10.1038/nature25019

- 13. Castledine M, Padfield D, Buckling A. Experimental (co)evolution in a multi-species microbial community results in local maladaptation. Ecol Lett. 2020;23: 1673–1681. doi:10/gsnpfz
- Varga JJ, Zhao CY, Davis JD, Hao Y, Farrell JM, Gurney JR, et al. Antibiotics Drive
   Expansion of Rare Pathogens in a Chronic Infection Microbiome Model. mSphere.
   2022;7: e00318-22. doi:10.1128/msphere.00318-22
- Alseth EO, Pursey E, Luján AM, McLeod I, Rollie C, Westra ER. Bacterial
   biodiversity drives the evolution of CRISPR-based phage resistance. Nature.
   2019;574: 549–552. doi:10.1038/s41586-019-1662-9
- 674 16. Piccardi P, Vessman B, Mitri S. Toxicity drives facilitation between 4 bacterial species. Proc Natl Acad Sci. 2019;116: 15979–15984.
  676 doi:10.1073/pnas.1906172116
- 17. Großkopf T, Soyer OS. Synthetic microbial communities. Curr Opin Microbiol. 2014;18: 72–77. doi:10.1016/j.mib.2014.02.002
- 18. De Roy K, Marzorati M, Van den Abbeele P, Van de Wiele T, Boon N. Synthetic microbial ecosystems: an exciting tool to understand and apply microbial communities: Synthetic microbial ecosystems. Environ Microbiol. 2014;16: 1472–1481. doi:10.1111/1462-2920.12343
- Karkaria BD, Manhart A, Fedorec AJH, Barnes CP. Chaos in synthetic microbial
   communities. PLOS Comput Biol. 2022;18: e1010548.
   doi:10.1371/journal.pcbi.1010548
- Wang T, Weiss A, Aqeel A, Wu F, Lopatkin AJ, David LA, et al. Horizontal gene transfer enables programmable gene stability in synthetic microbiota. Nat Chem Biol. 2022; 1–8. doi:10.1038/s41589-022-01114-3
- 21. Dion MB, Oechslin F, Moineau S. Phage diversity, genomics and phylogeny. Nat Rev Microbiol. 2020;18: 125–138. doi:10.1038/s41579-019-0311-5
- 691 22. Suttle CA. Viruses in the sea. Nature. 2005;437: 356–361. doi:10.1038/nature04160
- Chevallereau A, Pons BJ, van Houte S, Westra ER. Interactions between bacterial
   and phage communities in natural environments. Nat Rev Microbiol. 2021; 1–14.
   doi:10.1038/s41579-021-00602-y
- 696 24. Sullivan MB, Weitz JS, Wilhelm S. Viral ecology comes of age. Environ Microbiol Rep. 2017;9: 33–35. doi:https://doi.org/10.1111/1758-2229.12504
- Fazzino L, Anisman J, Chacón JM, Heineman RH, Harcombe WR. Lytic
   bacteriophage have diverse indirect effects in a synthetic cross-feeding community.
   ISME J. 2020;14: 123–134. doi:10.1038/s41396-019-0511-z

- Castledine M, Sierocinski P, Inglis M, Kay S, Hayward A, Buckling A, et al. Greater
   Phage Genotypic Diversity Constrains Arms-Race Coevolution. Front Cell Infect
   Microbiol. 2022;12: 834406. doi:10.3389/fcimb.2022.834406
- 704 27. Morella NM, Gomez AL, Wang G, Leung MS, Koskella B. The impact of 705 bacteriophages on phyllosphere bacterial abundance and composition. Mol Ecol. 706 2018;27: 2025–2038. doi:10.1111/mec.14542
- 707 28. Tecon R, Mitri S, Ciccarese D, Or D, van der Meer JR, Johnson DR. Bridging the 708 Holistic-Reductionist Divide in Microbial Ecology. mSystems. 2019;4: e00265-18, 709 /msystems/4/1/msys.00265-18.atom. doi:10.1128/mSystems.00265-18
- 29. Blazanin M, Turner PE. Community context matters for bacteria-phage ecology and evolution. ISME J. 2021; 1–10. doi:10.1038/s41396-021-01012-x
- 712 30. Clooney AG, Sutton TDS, Shkoporov AN, Holohan RK, Daly KM, O'Regan O, et al.
   713 Whole-Virome Analysis Sheds Light on Viral Dark Matter in Inflammatory Bowel
   714 Disease. Cell Host Microbe. 2019;26: 764-778.e5. doi:10.1016/j.chom.2019.10.009
- 715 31. Norman JM, Handley SA, Baldridge MT, Droit L, Liu CY, Keller BC, et al. Disease-716 Specific Alterations in the Enteric Virome in Inflammatory Bowel Disease. Cell. 717 2015;160: 447–460. doi:10.1016/j.cell.2015.01.002
- 32. Zuo T, Lu X-J, Zhang Y, Cheung CP, Lam S, Zhang F, et al. Gut mucosal virome alterations in ulcerative colitis. Gut. 2019;68: 1169–1179. doi:10.1136/gutjnl-2018-318131
- 33. Ma Y, You X, Mai G, Tokuyasu T, Liu C. A human gut phage catalog correlates the gut phageome with type 2 diabetes. Microbiome. 2018;6: 24. doi:10.1186/s40168-018-0410-y
- 34. Tetz G, Brown SM, Hao Y, Tetz V. Parkinson's disease and bacteriophages as its overlooked contributors. Sci Rep. 2018;8: 10812. doi:10.1038/s41598-018-29173-4
- 35. Mirzaei MK, Khan MAA, Ghosh P, Taranu ZE, Taguer M, Ru J, et al.
   Bacteriophages Isolated from Stunted Children Can Regulate Gut Bacterial
   Communities in an Age-Specific Manner. Cell Host Microbe. 2020;27: 199-212.e5.
   doi:10.1016/j.chom.2020.01.004
- 730 36. Mayo-Muñoz D, Pinilla-Redondo R, Birkholz N, Fineran PC. A host of armor:
   731 Prokaryotic immune strategies against mobile genetic elements. Cell Rep. 2023;42.
   732 doi:10.1016/j.celrep.2023.112672
- 37. Georjon H, Bernheim A. The highly diverse antiphage defence systems of bacteria.
  Nat Rev Microbiol. 2023; 1–15. doi:10.1038/s41579-023-00934-x
- 38. Labrie SJ, Samson JE, Moineau S. Bacteriophage resistance mechanisms. Nat Rev Microbiol. 2010;8: 317–327. doi:10.1038/nrmicro2315

- 39. Bikard D, Marraffini LA. Innate and adaptive immunity in bacteria: mechanisms of programmed genetic variation to fight bacteriophages. Curr Opin Immunol.
- 739 2012;24: 15–20. doi:10.1016/j.coi.2011.10.005
- 740 40. Rostøl JT, Marraffini L. (Ph)ighting Phages: How Bacteria Resist Their Parasites.
   741 Cell Host Microbe. 2019;25: 184–194. doi:10.1016/j.chom.2019.01.009
- 742 41. Dimitriu T, Szczelkun MD, Westra ER. Evolutionary Ecology and Interplay of
   743 Prokaryotic Innate and Adaptive Immune Systems. Curr Biol CB. 2020;30: R1189–
   744 R1202. doi:10.1016/j.cub.2020.08.028
- 42. Harvey H, Bondy-Denomy J, Marquis H, Sztanko KM, Davidson AR, Burrows LL.
   Pseudomonas aeruginosa defends against phages through type IV pilus glycosylation. Nat Microbiol. 2018;3: 47–52. doi:10.1038/s41564-017-0061-y
- 748 43. Barrangou R, Fremaux C, Deveau H, Richards M, Boyaval P, Moineau S, et al.
   749 CRISPR Provides Acquired Resistance Against Viruses in Prokaryotes. Science.
   750 2007;315: 1709–1712. doi:10.1126/science.1138140
- 44. Laanto E, Bamford JKH, Laakso J, Sundberg L-R. Phage-Driven Loss of Virulence
   in a Fish Pathogenic Bacterium. Brockhurst MA, editor. PLoS ONE. 2012;7:
   e53157. doi:10.1371/journal.pone.0053157
- 45. León M, Bastías R. Virulence reduction in bacteriophage resistant bacteria. Front
   Microbiol. 2015;6. doi:10.3389/fmicb.2015.00343
- 46. Hosseinidoust Z, Tufenkji N, van de Ven TGM. Formation of biofilms under phage
   predation: considerations concerning a biofilm increase. Biofouling. 2013;29: 457–
   468. doi:10.1080/08927014.2013.779370
- 759 47. Chan BK, Sistrom M, Wertz JE, Kortright KE, Narayan D, Turner PE. Phage
   760 selection restores antibiotic sensitivity in MDR Pseudomonas aeruginosa. Sci Rep.
   761 2016;6: 26717. doi:10.1038/srep26717
- 48. Bhargava N, Sharma P, Capalash N. Pyocyanin Stimulates Quorum Sensing Mediated Tolerance to Oxidative Stress and Increases Persister Cell Populations in
   Acinetobacter baumannii. McCormick BA, editor. Infect Immun. 2014;82: 3417–
   3425. doi:10.1128/IAI.01600-14
- 766 49. Drevinek P, Mahenthiralingam E. Burkholderia cenocepacia in cystic fibrosis:
   767 epidemiology and molecular mechanisms of virulence. Clin Microbiol Infect.
   768 2010;16: 821–830. doi:10.1111/j.1469-0691.2010.03237.x
- 769 50. Pendleton JN, Gorman SP, Gilmore BF. Clinical relevance of the ESKAPE
   770 pathogens. Expert Rev Anti Infect Ther. 2013;11: 297–308. doi:10.1586/eri.13.12

- 51. Stacy A, McNally L, Darch SE, Brown SP, Whiteley M. The biogeography of polymicrobial infection. Nat Rev Microbiol. 2016;14: 93–105.
- 773 doi:10.1038/nrmicro.2015.8
- 774 52. Thingstad TF. Elements of a theory for the mechanisms controlling abundance, diversity, and biogeochemical role of lytic bacterial viruses in aquatic systems.
- 776 Limnol Oceanogr. 2000;45: 1320–1328. doi:10.4319/lo.2000.45.6.1320
- 53. de Roode JC, Culleton R, Bell AS, Read AF. Competitive release of drug
   resistance following drug treatment of mixed Plasmodium chabaudi infections.
   Malar J. 2004;3: 33. doi:10.1186/1475-2875-3-33
- Wale N, Sim DG, Jones MJ, Salathe R, Day T, Read AF. Resource limitation
   prevents the emergence of drug resistance by intensifying within-host competition.
   Proc Natl Acad Sci. 2017;114: 13774–13779. doi:10.1073/pnas.1715874115
- 783 55. Wollein Waldetoft K, Sundius S, Kuske R, Brown SP. Defining the Benefits of
   784 Antibiotic Resistance in Commensals and the Scope for Resistance Optimization.
   785 mBio. 2022;14: e01349-22. doi:10.1128/mbio.01349-22
- 786 56. Persat A, Inclan YF, Engel JN, Stone HA, Gitai Z. Type IV pili mechanochemically 787 regulate virulence factors in *Pseudomonas aeruginosa*. Proc Natl Acad Sci. 788 2015;112: 7563–7568. doi:10.1073/pnas.1502025112
- 57. Lloyd-Smith JO. Vacated niches, competitive release and the community ecology
   of pathogen eradication. Philos Trans R Soc B Biol Sci. 2013;368: 20120150.
   doi:10.1098/rstb.2012.0150
- 58. Lenski RE, Rose MR, Simpson SC, Tadler SC. Long-Term Experimental Evolution
   in Escherichia coli. I. Adaptation and Divergence During 2,000 Generations. Am
   Nat. 1991;138: 1315–1341. doi:10.1086/285289
- 795 59. Travisano M, Lenski RE. Long-Term Experimental Evolution in Escherichia coli. IV. 796 Targets of Selection and the Specificity of Adaptation. Genetics. 1996;143: 15–26. 797 doi:10.1093/genetics/143.1.15
- 798 60. Mounier J, Monnet C, Vallaeys T, Arditi R, Sarthou A-S, Hélias A, et al. Microbial Interactions within a Cheese Microbial Community. Appl Environ Microbiol. 2008;74: 172–181. doi:10.1128/AEM.01338-07
- 801 61. Buffie CG, Bucci V, Stein RR, McKenney PT, Ling L, Gobourne A, et al. Precision 802 microbiome reconstitution restores bile acid mediated resistance to Clostridium 803 difficile. Nature. 2015;517: 205–208. doi:10.1038/nature13828
- 804 62. Venturelli OS, Carr AV, Fisher G, Hsu RH, Lau R, Bowen BP, et al. Deciphering 805 microbial interactions in synthetic human gut microbiome communities. Mol Syst 806 Biol. 2018;14: e8157. doi:10.15252/msb.20178157

- Liao C, Xavier JB, Zhu Z. Enhanced inference of ecological networks by
   parameterizing ensembles of population dynamics models constrained with prior
   knowledge. BMC Ecol. 2020;20: 3. doi:10.1186/s12898-019-0272-6
- 810 64. Widder S, Allen RJ, Pfeiffer T, Curtis TP, Wiuf C, Sloan WT, et al. Challenges in 811 microbial ecology: building predictive understanding of community function and 812 dynamics. ISME J. 2016;10: 2557–2568. doi:10.1038/ismej.2016.45
- 813 65. Wootton JT. The Nature and Consequences of Indirect Effects in Ecological Communities. 1994. doi:10/dzfmpb
- 815 66. VanEvery H, Franzosa EA, Nguyen LH, Huttenhower C. Microbiome epidemiology 816 and association studies in human health. Nat Rev Genet. 2023;24: 109–124. 817 doi:10.1038/s41576-022-00529-x
- 67. Petersen C, Round JL. Defining dysbiosis and its influence on host immunity and disease. Cell Microbiol. 2014;16: 1024–1033. doi:10.1111/cmi.12308
- 820 68. Waller AS, Yamada T, Kristensen DM, Kultima JR, Sunagawa S, Koonin EV, et al.
  821 Classification and quantification of bacteriophage taxa in human gut metagenomes.
  822 ISME J. 2014;8: 1391–1402. doi:10.1038/ismej.2014.30
- 69. Dahlman S, Avellaneda-Franco L, Barr JJ. Phages to shape the gut microbiota? Curr Opin Biotechnol. 2021;68: 89–95. doi:10.1016/j.copbio.2020.09.016
- 70. Sweere JM, Van Belleghem JD, Ishak H, Bach MS, Popescu M, Sunkari V, et al. Bacteriophage trigger antiviral immunity and prevent clearance of bacterial infection. Science. 2019;363: eaat9691. doi:10.1126/science.aat9691
- 71. Coyte KZ, Schluter J, Foster KR. The ecology of the microbiome: Networks, competition, and stability. Science. 2015;350: 663–666. doi:10.1126/science.aad2602
- Hofbauer J, Sigmund K. On the stabilizing effect of predators and competitors on ecological communities. J Math Biol. 1989;27: 537–548. doi:10.1007/BF00288433
- 73. Coyte KZ, Rao C, Rakoff-Nahoum S, Foster KR. Ecological rules for the assembly of microbiome communities. PLoS Biol. 2021;19: e3001116.
  doi:10.1371/journal.pbio.3001116
- 74. Bairey E, Kelsic ED, Kishony R. High-order species interactions shape ecosystem diversity. Nat Commun. 2016;7: 12285. doi:10.1038/ncomms12285
- 75. Grilli J, Barabás G, Michalska-Smith MJ, Allesina S. Higher-order interactions stabilize dynamics in competitive network models. Nature. 2017;548: 210–213. doi:10.1038/nature23273

- 76. Bucci V, Tzen B, Li N, Simmons M, Tanoue T, Bogart E, et al. MDSINE: Microbial Dynamical Systems INference Engine for microbiome time-series analyses.
- 843 Genome Biol. 2016;17: 121. doi:10.1186/s13059-016-0980-6
- 77. van Houte S, Ekroth AKE, Broniewski JM, Chabas H, Ashby B, Bondy-Denomy J, et al. The diversity-generating benefits of a prokaryotic adaptive immune system.
- 846 Nature. 2016;532: 385–388. doi:10.1038/nature17436
- 78. Westra ER, van Houte S, Oyesiku-Blakemore S, Makin B, Broniewski JM, Best A, et al. Parasite Exposure Drives Selective Evolution of Constitutive versus Inducible Defense. Curr Biol. 2015;25: 1043–1049. doi:10.1016/j.cub.2015.01.065
- 850 79. Meaden S, Capria L, Alseth E, Gandon S, Biswas A, Lenzi L, et al. Phage gene 851 expression and host responses lead to infection-dependent costs of CRISPR 852 immunity. ISME J. 2020; 1–10. doi:10.1038/s41396-020-00794-w
- 853 80. Goto M, Takahashi H, Segawa Y, Hayashidani H, Takatori K, Hara-Kudo Y. Real-854 Time PCR Method for Quantification of Staphylococcus aureus in Milk. J Food 855 Prot. 2007;70: 90–96. doi:10.4315/0362-028X-70.1.90
- 81. Davis JD, Olivença DV, Brown SP, Voit EO. Methods of quantifying interactions 857 among populations using Lotka-Volterra models. Front Syst Biol. 2022;2. Available: 858 https://www.frontiersin.org/articles/10.3389/fsysb.2022.1021897
- 859 82. Lenth RV. Least-Squares Means: The R Package Ismeans. J Stat Softw. 2016;69: 1–33. doi:10.18637/jss.v069.i01
- 83. R Core Team. R: A language and environment for statistical computing. R
  Foundation for Statistical Computing, Vienna, Austria. 2020. Available:
  https://www.R-project.org/
- 84. Wickham H, Averick M, Bryan J, Chang W, McGowan LD, François R, et al.
  Welcome to the Tidyverse. J Open Source Softw. 2019;4: 1686.
  doi:10.21105/joss.01686

867

Supplemental Fig 1. Line plot of bacterial densities in the absence of P. aeruginosa and its phage. Showing the bacterial densities in cfu/mL over time for SA (S. aureus), AB (A. baumannii), and BC (B. cenocepacia) in various co-culture combinations in the absence of P. aeruginosa and its phage. Dashed horizontal line at  $10^2$  cfu/mL marks the threshold of reliable detection where the qPCR results indicate the bacteria has gone or is close to extinction from a population. Data are mean  $\pm$  95% CI.

**Supplemental Fig 2. Ordination plot in the absence of phage.** PCA ordination of relative bacterial abundance in the absence of phage DMS3vir, with grid layouts separated into days post phage infection. Outer circle colour indicates which PA14 clone is present in the population, while inner circle indicates community composition (SA = S. aureus, AB = A. baumannii, BC = B. cenocepacia).

Supplemental Fig 3. Line plots of bacterial densities in the absence of phage. Showing the bacterial densities in cfu/mL over time for the PA14 WT and CRISPR-KO P. aeruginosa strains, and  $\mathbf{b}$  the other microbial community species (SA = S. aureus, AB = A. baumannii, BC = B. cenocepacia, MC = microbial community) in the absence of phage DMS3vir. Dashed horizontal line at  $10^2$  cfu/mL marks the threshold of reliable detection where the qPCR results indicate the bacteria has gone or is close to extinction from a population. Data are mean  $\pm$  95% CI.

Supplemental Fig 4. Line plots of bacterial densities in the presence of phage.

Showing the bacterial densities in cfu/mL over time for the PA14 WT and CRISPR-KO *P*.

aeruginosa strains, and **b** the other microbial community species (SA = S. aureus, AB = A. baumannii, BC = B. cenocepacia, MC = Microbial community) in the presence of phage DMS3vir. Dashed horizontal line at  $10^2$  cfu/mL marks the threshold of reliable detection where the qPCR results indicate the bacteria has gone or is close to extinction from a population. Data are mean  $\pm$  95% CI.

**Supplemental Fig 5. Ordination plots in the presence of phage.** PCA ordination of relative bacterial abundance in the presence of phage DMS3vir, with grid layouts separated into days post phage infection. Outer circle colour indicates which PA14 clone is present in the population, while inner circle indicates community composition (SA = S. aureus, AB = A. baumannii, BC = B. cenocepacia).

Supplemental Fig 6. Model from no phage data, trained on only pairwise experimental data. Model fit predictions for two-, three-, and full four species community dynamics (solid lines) compared to experimental data (dashed lines) (PA = P. aeruginosa, SA = S. aureus, AB = A. baumannii, BC = B. cenocepacia). Models were parameterized via optimization with least-squares to fit a system of ODEs (defined as a generalized Lotka-Volterra competition model with n species, where n=1,2,3,4). We parameterize the models via fitting of 1- (for growth rates  $r_i$ ) and 2- (for all possible pairwise interaction coefficients  $\beta_{i,j} \ \forall i,j=1,2$ ) species dynamics and use the resulting coefficients to predict the 3- and 4-species community dynamics. For fitting co-culture data, growth rates  $r_i$  were fixed from mono-culture data and interaction parameters  $\beta_{i,j}$  were all open. See Methods and Text S1 for a detailed description of mathematical modelling.

**Supplemental Fig 7. Long time simulation of full community model shows shift in ecological outcomes given inclusion of phage.** Simulation of the 4-species community gLV model over a long time scale reveals a qualitative shift in the outcome of the community when phage is present (PA = P. aeruginosa, SA = S. aureus, AB = A. baumannii, BC = B. cenocepacia). In the absence of phage (top), P. aeruginosa is the dominant competitor and only surviving species. In the presence of phage (bottom), the dominant competitor is eliminated, and we see competitive release of A. baumannii and S. aureus — maintaining 2 of the 3 non-targeted species in the community. Growth and interaction coefficients for simulation are from the model fits in Figures 9 and 10, and are shown for the wild-type PA14, no phage case (top left) in Fig. S8. For a detailed description of model parameterization and simulation methods, see Methods and Text S1.

**Supplemental Fig 8.** Inferred interaction coefficients for the fitted gLV model describing full community dynamics, using 2- and 3-species experimental data with wildtype PA14 in the absence of phage (Fig. 9) (PA = P. aeruginosa, SA = S. aureus, AB = A. baumannii, BC = B. cenocepacia). Heat map depicts  $\beta_{i,j}$  coefficients (also labelled) scaled by P. aeruginosa intraspecific competition ( $\beta_{1,1} = 1.2617 \times 10^{-8}$ , top left) corresponding to the wildtype PA14 case in Fig. 9 (see Fig. 9, Methods, and Text S1 for a description of model fitting methods). The x-axis represents species j (the actor) and the y-axis represents species i (the recipient) where  $\beta_{i,j}$  describes the per capita inhibitory effect of species j

on species i. Colour bar ranges from neutral (or no) interaction ( $\beta_{i,j} = 0$ , white) to strong inhibition (red).